Virology 483 (2015) 203–208

Contents lists available at ScienceDirect

Virology

journal homepage: www.elsevier.com/locate/yviro

# The sweet quartet: Binding of fucose to the norovirus capsid

Anna D. Koromyslova [a,b,1], Mila M. Leuthold [a,b,1], Matthew W. Bowler [c,d], Grant S. Hansman [a,b,*]

[a] Schaller Research Group at the University of Heidelberg and the DKFZ, Heidelberg 69120, Germany
[b] Department of Infectious Diseases, Virology, University of Heidelberg, Heidelberg 69120, Germany
[c] European Molecular Biology Laboratory, Grenoble Outstation, 71 Avenue des Martyrs, CS 90181, Grenoble, F-38042, France
[d] Unit for Virus Host Cell Interactions, Univ. Grenoble Alpes-EMBL-CNRS, 71 Avenue des Martyrs, CS 90181, Grenoble F-38042, France

ARTICLE INFO

*Article history:*
Received 28 February 2015
Returned to author for revisions
24 March 2015
Accepted 7 April 2015
Available online 15 May 2015

*Keywords:*
Norovirus
Histo-blood group antigens (HBGAs)
Capsid
Fucose

ABSTRACT

Human noroviruses bind histo-blood group antigens (HBGAs) and this interaction is thought to be important for an infection. We identified two additional fucose-binding pockets (termed fucose-3/4 sites) on a genogroup II human (GII.10) norovirus-protruding (P) dimer using X-ray crystallography. Fucose-3/4 sites were located between two previously determined HBGA binding pockets (termed fucose-1/2 sites). We found that four fucose molecules were capable of binding altogether at fucose-1/2/3/4 sites on the P dimer, though the fucose molecules bound in a dose-dependent and step-wise manner. We also showed that HBGA B-trisaccharide molecules bound in a similar way at the fucose-1/2 sites. Interestingly, we discovered that the monomers of the P dimer were asymmetrical in an unliganded state and when a single B-trisaccharide molecule bound, but were symmetrical when two B-trisaccharide molecules bound. We postulate that the symmetrical dimers might favor HBGA binding interactions at fucose-1/2 sites.



## Introduction

Human noroviruses are the dominant cause of acute gastroenteritis. Noroviruses are genetically and antigenically distinct with two main genogroups (GI and GII) causing the majority of infections in humans. The norovirus capsid protein is divided into the shell (S) and protruding (P) domains, the latter of which is further subdivided into P1 and P2 subdomains (Prasad et al., 1999). Noroviruses bind histo-blood group antigens (HBGAs), which are polymorphic carbohydrate structures present as free antigens in saliva and found on the surface of various epithelia. Interestingly, HBGA binding was found to enhance norovirus infection in cell culture (Jones et al., 2014). Noroviruses bind HBGAs on the P domain, where GI noroviruses have a monomeric interaction with HBGAs and GII noroviruses have a dimeric interaction (Hansman et al., 2011; Cao et al., 2007; Bu et al., 2008). At least nine different HBGA types have been recognized to bind to noroviruses and these are typically grouped into either ABH or Lewis types that are distinguished by the different connections of a fucose moiety. The ABH types are characterized by an α-L-fucose-(1-2)-β-D-galactose connection, whereas the Lewis types contain an α-L-fucose-(1-3)/(1-4)-β-D-*N*-acetyl-glucosamine. The GII noroviruses primarily interact with the ABH-fucose, Lewis-fucose, or a combination of both. The fucose moiety of the HBGAs is usually held firmly by a common set of GII P domain residues, whereas the other saccharide units are held less firmly with variable residues and water-mediated interactions (Hansman et al., 2011; Singh et al., 2015).

In this study, we investigated a concentration-dependent binding of L-fucose-monosaccharide (fucose) and B-trisaccharide (B-tri) to the GII genotype 10 (GII.10) norovirus P dimer using X-ray crystallography. We identified two additional fucose-binding pockets and showed that four fucose moieties were bound per dimer. We also found that fucose and B-tri bound in a dose-dependent and step-wise manner.

## Results and discussion

Molecular replacement indicated a P dimer in space group $P2_1$ for all datasets. Data statistics are shown in Tables 1 and 2. All P domain complexes were reminiscent of the previously published unliganded GII.10 P domain structure (Fig. 1A) (Hansman et al., 2011). Co-crystallization at 300 mM and 150 mM of fucose revealed four clearly discernable patches of fucose electron density

* Correspondence to: CHS Foundation, University of Heidelberg, and DKFZ. Norovirus Study Group. Im Neuenheimer Feld 242, Heidelberg 69120, Germany.
*E-mail address:* g.hansman@dkfz.de (G.S. Hansman).
[1] Equal contribution.

http://dx.doi.org/10.1016/j.virol.2015.04.006
0042-6822/

**Table 1**
Data collection and refinement statistics of GII.10 P domain fucose complex structures.

| | GII.10-Fucose$^{300\ mM}$ (4Z4R) | GII.10-Fucose$^{150\ mM}$ (4Z4S) | GII.10-Fucose$^{75\ mM}$ (4Z4T) | GII.10-Fucose$^{37.5\ mM}$ (4Z4U) | GII.10-Fucose$^{19\ mM}$ (4Z4V) | GII.10-Fucose$^{4.7\ mM}$ (4Z4W) |
|---|---|---|---|---|---|---|
| Data collection | | | | | | |
| Space group | $P2_1$ | $P2_1$ | $P2_1$ | $P2_1$ | $P2_1$ | $P2_1$ |
| Cell dimensions | | | | | | |
| *a*, *b*, *c* (Å) | 66.10 78.94 68.89 | 66.09 78.68 68.81 | 65.75 78.85 68.64 | 65.32 78.77 68.51 | 65.11 78.82 68.66 | 65.29 79.34 69.58 |
| α, β, γ (°) | 90 99.84 90 | 90 99.61 90 | 90 99.43 90 | 90 99.52 90 | 90 99.77 90 | 90 100.78 90 |
| Resolution range (Å) | 43.44–1.80 | 43.08–1.80 | 43.42–1.80 | 43.19–1.88 | 43.05–1.80 | 43.41–1.80 |
| | (1.87–1.80)[a] | (1.86–1.80)[a] | (1.86–1.80)[a] | (1.95–1.88)[a] | (1.86–1.80)[a] | (1.86–1.80)[a] |
| $R_{sym}$ | 3.96 (17.11)[a] | 6.39 (29.73)[a] | 4.43 (18.71)[a] | 7.84 (60.84)[a] | 4.9 (38.16)[a] | 7.01 (23.37)[a] |
| $I/\sigma I$ | 21.91 (6.59)[a] | 13.76 (4.06)[a] | 18.25 (5.97)[a] | 11.56 (1.81)[a] | 16.73 (3.02)[a] | 16.62 (5.99)[a] |
| Completeness (%) | 99.26 (95.78)[a] | 99.01 (97.40)[a] | 98.79 (96.05)[a] | 98.92 (95.03)[a] | 98.81 (95.10)[a] | 98.66 (94.29)[a] |
| Redundancy | 3.4 (3.3)[a] | 3.2 (3.2)[a] | 3.1 (2.8)[a] | 3.0 (2.9)[a] | 2.9 (2.9)[a] | 3.0 (2.8)[a] |
| Refinement | | | | | | |
| Resolution range (Å) | 43.44–1.80 | 43.08–1.80 | 43.42–1.80 | 43.19–1.88 | 43.05–1.80 | 43.41–1.80 |
| No. of reflections | 64050 | 63885 | 63487 | 54695 | 62731 | 63970 |
| $R_{work}/R_{free}$ | 0.14/0.17 | 0.14/0.18 | 0.15/0.17 | 0.16/0.20 | 0.15/0.18 | 0.15/0.19 |
| No. of atoms | 5690 | 5664 | 5535 | 5366 | 5454 | 5643 |
| Protein | 4893 | 4847 | 4767 | 4768 | 4790 | 4806 |
| Ligand/ion | 64 | 80 | 72 | 58 | 39 | 23 |
| Water | 733 | 737 | 696 | 540 | 625 | 814 |
| Average *B* factors (Å$^2$) | | | | | | |
| Protein | 18.70 | 17.00 | 20.00 | 27.40 | 24.10 | 16.10 |
| Ligand/ion | 18.70 | 17.20 | 24.50 | 31.20 | 26.50 | 20.40 |
| Water | 30.70 | 29.40 | 31.10 | 35.80 | 34.60 | 28.40 |
| RMSD | | | | | | |
| Bond length (Å) | 0.014 | 0.015 | 0.008 | 0.008 | 0.011 | 0.008 |
| Bond angle (°) | 1.42 | 1.43 | 1.14 | 1.06 | 1.29 | 1.15 |

Each data set was collected from single crystals, respectively.
[a] Values in parentheses are for highest-resolution shell.

**Table 2**
Data collection and refinement statistics of GII.10 P domain B-tri complex structures.

| | GII.10-Btri$^{30\ mM}$ (4Z4Z) | GII.10-Btri$^{7.5\ mM}$ (4Z4Y) |
|---|---|---|
| Data collection | | |
| Space group | $P2_1$ | $P2_1$ |
| Cell dimensions | | |
| *a*, *b*, *c* (Å) | 66.83 78.29 71.63 | 65.12 78.67 69.77 |
| α, β, γ (°) | 90 103.35 90 | 90 100.36 90 |
| Resolution range (Å) | 42.86–1.80 | 43.2–1.80 |
| | (1.86–1.80)[a] | (1.86–1.80)[a] |
| $R_{sym}$ | 6.86 (50.46)[a] | 4.78 (20.84)[a] |
| $I/\sigma I$ | 11.57 (2.14)[a] | 18.00 (6.12)[a] |
| Completeness (%) | 98.88 (95.13)[a] | 99.08 (95.54)[a] |
| Redundancy | 3.0 (3.0)[a] | 2.3 (3.1)[a] |
| Refinement | | |
| Resolution range (Å) | 42.86–1.80 | 43.20–1.80 |
| No. of reflections | 65787 | 63976 |
| $R_{work}/R_{free}$ | 0.16/0.19 | 0.14/0.18 |
| No. of atoms | 5426 | 5457 |
| Protein | 4805 | 4809 |
| Ligand/ion | 94 | 69 |
| Water | 527 | 579 |
| Average *B* factors (Å$^2$) | | |
| Protein | 21.70 | 18.30 |
| Ligand/ion | 25.30 | 21.80 |
| Water | 28.00 | 27.60 |
| RMSD | | |
| Bond length (Å) | 0.007 | 0.010 |
| Bond angle (°) | 1.06 | 1.24 |

Each data set was collected from single crystals, respectively.
[a] Values in parentheses are for highest-resolution shell.

(Fig. 1A and B). Two electron density patches corresponded to fucose molecules at the HBGA binding sites as previously described (hereafter termed fucose-1 and fucose-2 sites) (Hansman et al., 2011). Two additional electron density patches, representing two fucose molecules (termed fucose-3 and fucose-4 sites), were located between fucose-1/2 sites. At 300 mM and 150 mM of fucose, the four-fucose electron density patches were equivalent, suggesting a similar occupancy at fucose-1/2/3/4 sites (Fig. 1B). At 75 mM of fucose, the electron density patches of fucose at fucose-1/2/3/4 sites were apparent, although fucose-3/4 electron densities were less distinct than the fucose-1/2 sites, indicating a weaker fucose binding at fucose-3/4 sites (Fig. 1B). At 37.5 mM of fucose, only fucose molecules at fucose-1/2 sites bound to the P dimer, since the electron densities at fucose-3/4 sites were lacking and as such fucose was not modeled into the structure (Fig. 1B). At 19 mM and 4.7 mM of fucose, only fucose-1 site was occupied (Fig. 1B).

These data indicated that fucose bound to the P dimer in a dose dependent manner and that binding occurred through a three-step binding process, i.e., firstly fucose-1 site, followed by fucose-2 site, and then simultaneously fucose-3/4 sites. Our data also indicated that fucose-3/4 sites were only occupied after binding at fucose-1/2 sites. Taken together, these new findings implied a cooperative binding of the fucose molecules on the P dimer, which might be associated with different affinities at fucose-1, fucose-2, and fucose 3/4 sites.

At fucose-1/2 sites, the fucose molecules were held at the dimeric interface by the regular set of P domain residues (Hansman et al., 2011). Direct interactions were provided with the side chains of Asn355, Asp385, and Arg356, the main chain of Gly451, and a hydrophobic interaction with Tyr452 (Fig. 1C). The

fucose molecules at fucose-3/4 sites were also held at the dimeric interface and residues from both monomers contributed to the binding (Fig. 1D). Direct hydrogen bonds were provided with the side chains of Glu359 and Lys449 from one monomer and water-mediated interactions were observed with the other monomer. A Pi-alkyl stacking and hydrophobic interaction with fucose and the indole ring of Trp381 was observed at fucose-3/4 sites (Fig. 1D). The stacking interaction of fucose with the indole ring of Trp is commonly present in other carbohydrate binding proteins and likely serves to position the saccharide in the binding site and enhance specificity (Wimmerova et al., 2012; Soisson et al., 1997). Interestingly, the fucose molecules at fucose-3/4 sites were connected by an additional hydrophobic interaction and a single water-mediated interaction. Seen in this way, the hydrophobic interactions appeared to cross-link $Trp381^{B\text{-}chain}$-$fucose^{fucose\text{-}3}$ to $fucose^{fucose\text{-}4}$-$Trp381^{A\text{-}chain}$, strengthened by the water-mediated interaction.

We previously showed that the GII.10 P dimer bound a single B-tri at fucose-1 site on the GII.10 P dimer at ~1 mM of B-tri (Hansman et al., 2011). In order to investigate the possibilities that B-tri also bound in a comparable dose-dependent manner as fucose, we examined two different concentrations of B-tri (30 mM and 7.5 mM) in complex with the GII.10 P domain. We found that two B-tri molecules bound at fucose-1/2 sites at 30 mM of B-tri and that one B-tri molecule bound at fucose-1 site at 7.5 mM of B-tri (Fig. 2A). The B-tri molecules were firmly held by the regular set of P dimer residues as previously described (Hansman et al., 2011), except for some minor differences (Fig. 2B). The terminal galactose at fucose-1 site did not form single-water-mediated interactions that were observed at fucose-2 site, although long distance double-water-mediated interactions were observed between the terminal galactose and P dimer (data not shown). These results indicated that B-tri also bound in a dose-dependent manner. Unfortunately, higher concentrations of B-tri in complex with the P dimer failed to crystallize, therefore, we could not determine if B-tri molecules were able to bind at fucose-3/4 sites.

Our novel results showed that fucose and B-tri molecules bound in a dose-dependent and step-wise binding process at fucose-1/2 sites. However, this finding was somewhat surprising, since the norovirus P domain was expected to form a symmetrical homodimer, implying that two fucose or two HBGA molecules could bind simultaneously at fucose-1/2 sites. Close inspection of the GII.10 P dimer chains A and B, revealed a loop near the fucose-1/2 sites in two alternative conformations, i.e., residues Val294-Thr301 (Fig. 2C). When one B-tri molecule bound to the P dimer, one loop was in an “up” position at the occupied fucose-1 site and the other loop was in a “down” position at the unoccupied fucose-2 site (Fig. 2C). When two B-tri molecules bound to the P dimer, both loops were at the “down” positions (Fig. 2C). Comparison with previous GII.10 P domain HBGA complex structures confirmed that this alternative conformation was present when only fucose-1 site was occupied (Hansman et al., 2011). These results indicated that the GII.10 P dimers in the unliganded state or with a single HBGA formed an asymmetrical homodimer, whereas P dimers with two B-tri molecules formed a symmetrical homodimer.

The reasons for the loop movement were not entirely clear, since the repositioned loop did not directly interact with the B-tri molecules. However, the loop movement and repositioning of side chains may have created a more favorable geometry surrounding the HBGA pocket for simultaneous HBGA binding. Indeed, we recently showed that three prevalent GII.4 noroviruses generally bind two HBGA molecules per dimer at lower HBGA concentrations (i.e., $<1$ mM) (Hansman et al., 2011; Singh et al., 2015; Hansman et al., 2012); and the equivalent loops in GII.4 were similarly positioned in the liganded and unliganded structures (Singh et al., 2015) These results also suggested that GII.4 P domains usually form symmetrical homodimers. Expanding from these observations, the fucose-1/2 sites in the prevalent GII.4 strains might be more optimized for simultaneous HBGA binding than in the rarely detected GII.10 strains. Considering that HBGA binding enhances norovirus infection in cell culture, simultaneous HBGA binding at lower concentrations may confer an infection advantage for viruses. However, further studies to verify these notions are required.

## Conclusions

We showed that the GII.10 P domain contained two additional fucose-binding sites. The biological relevance of the fucose-3/4 sites is currently unknown. However, the higher concentration of fucose required for binding at fucose-3/4 sites suggested a weaker affinity than the fucose-1/2 sites, which was reported in the low millimolar range (Hansman et al., 2012). The low affinity for fucose at a single binding site might be compensated by a cluster of several fucose binding sites on one P dimer as previously shown for lectin-carbohydrate recognition (Noble et al., 2009). Moreover, a local high concentration of fucose-containing molecules, e.g., on lipid rafts, could enhance simultaneous binding at fucose-1/2/3/4 sites (Noble et al., 2009; Lundquist and Toone, 2002). Taken together, these novel findings showed that four fucose molecules formed a sweet quartet on the GII.10 P dimer through cooperative binding.

## Materials and methods

The GII.10 P domain was expressed and purified as previously described (Hansman et al., 2011). Briefly, the near-full length GII.10 P domain was optimized for *Escherichia coli* expression and cloned into a modified His-tagged pMal-c2x vector at the BamHI and NotI (New England Biolabs) restriction sites. The pMal-c2x-P domain plasmid was transformed into BL21 cells (Invitrogen) for protein expression. Expression was induced with IPTG (1 mM) for 18 h at 22 °C. The His-tagged fusion-P domain protein was purified from a Ni column (Qiagen), digested with HRV-3C protease overnight at 4 °C, and the P domain separated on the Ni column. The P domain was further purified by size exclusion chromatography with a Superdex 200 column (GE) and concentrated to 2.5 mg/ml and stored in gel filtration buffer (0.35 M NaCl and 2.5 mM Tris pH 7.0).

L-fucose (fucose; Dextra, UK) was serially diluted in distilled water from a starting concentration of 600 mM. The same batch of GII.10 P domain was mixed 1:1 in the crystallization mother liquor [0.2 M sodium nitrate, 0.1 bis-tris propane (pH 7.5), and 20% (w/v) PEG3350] and then 5 μl of this mixture was added to 5 μl of each fucose dilution. One microliter drops of P domain-fucose were applied to crystallization wells and crystals were grown for ten days at 18 °C. Six (final) concentrations of fucose in complex with the GII.10 P domain were analyzed (300 mM, 150 mM, 75 mM, 37.5 mM, 19 mM, and 4.7 mM). Similarly, we co-crystallized two different concentrations of B-tri (30 mM and 7.5 mM) (Dextra, UK) in complex with the GII.10 P domain. The fucose and B-tri concentrations were considerably higher than our previous HBGA concentrations, i.e., ~1 mM (Hansman et al., 2011; Singh et al., 2015; Hansman et al., 2012). Prior to flash freezing, crystals of similar size were transferred to a mother liquor containing 30% ethylene glycol and corresponding fucose/B-tri concentrations. X-ray diffraction data were collected at the European Synchrotron Radiation Facility, France MASSIF-1 (ID30A-1) using automatic routines for data collection (Bowler et al., 2010; Brockhauser

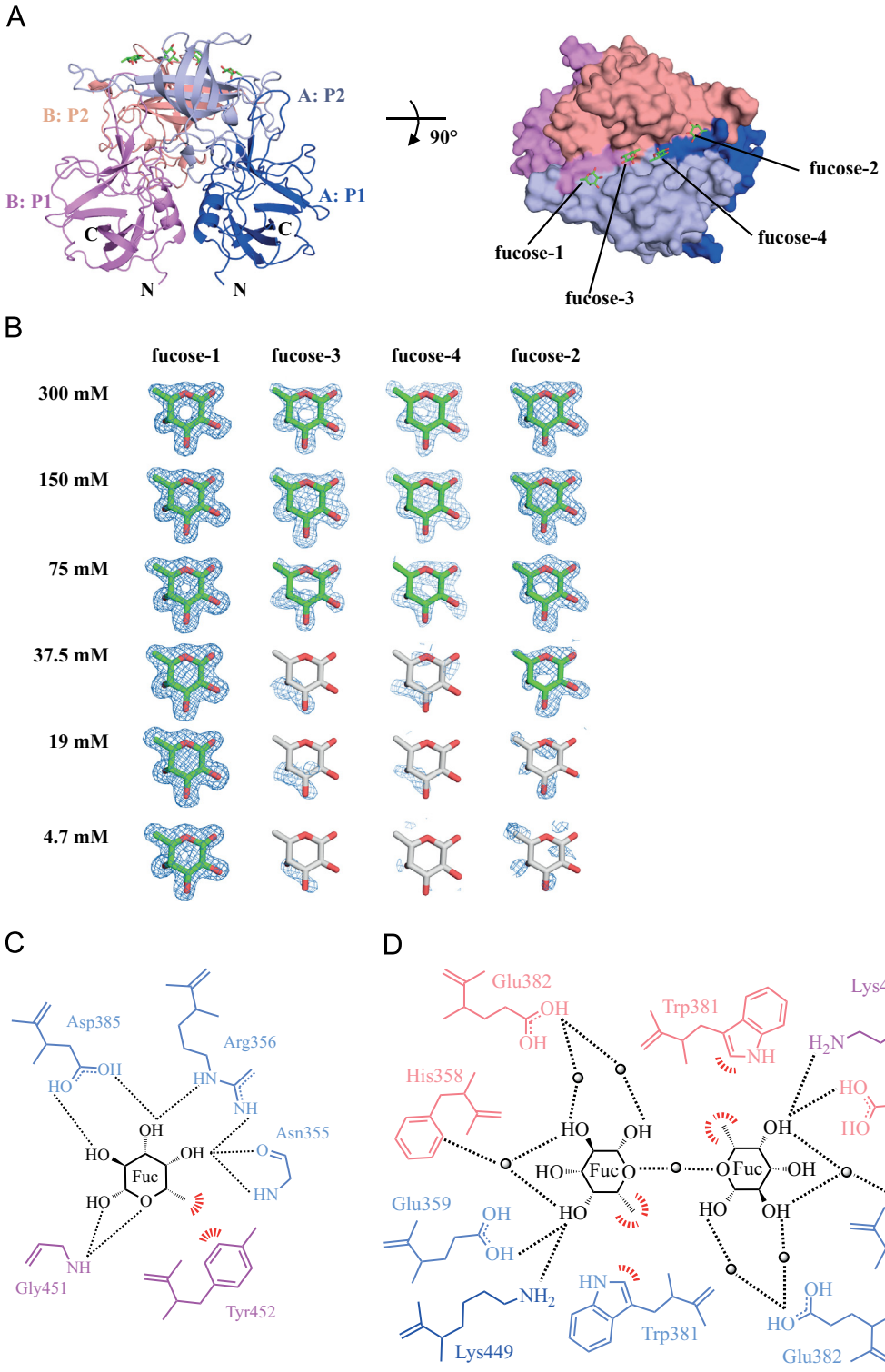


**Fig. 1.** GII.10 P domain binding interaction with fucose. (A) Structure of the GII.10 P domain–fucose complex (P dimer, cartoon and surface representation; fucose, sticks). The X-ray crystal structure of the GII.10 P domain–fucose complex was determined to 1.8 Å resolution. The complex was colored according to GII.10 P domain monomers (chain A and B) and P1 and P2 subdomains, i.e., chain A: P1 (blue), chain A: P2 (light blue), chain B: P1 (violet), chain B: P2 (salmon), and fucose (green). The surface representation (right) shows the fucose binding at the dimeric interface. (B) Dose-dependent binding of fucose to the P dimer. The simulated annealing $F_o - F_c$ omit map (blue) was contoured at 2.5$\sigma$. The hydroxyl group at C1 in the fucose was fixed in the β-position in all structures. At all dilutions, fucose-1 electron density was clearly defined. At 300 mM and 150 mM of fucose, the electron densities were clearly distinguishable at fucose-1/2/3/4 sites, indicating that all four fucoses bound strongly to the P dimer. At 75 mM of fucose, four fucose molecules bound at fucose-1/2/3/4. At 37 mM, fucose molecules at fucose-3/4 sites (white sticks) were considered not bound. At 19 mM and 4.7 mM, fucose molecules at fucose-2/3/4 sites (white sticks) were considered not bound. (C) Fucose (Fuc) at fucose-1 site was held with a network of binding interactions (colored as A). The fucose was held by direct hydrogen bonds (black dashes) with the side chains of Asn355$^{\text{chain-A}}$, Arg356$^{\text{chain-A}}$, and Asp385$^{\text{chain-A}}$, and with the main chain of Gly451$^{\text{chain-B}}$. A hydrophobic interaction (red dashes) with the fucose was provided with the aromatic ring of Tyr452$^{\text{chain-B}}$. Water-mediated interactions were also observed (not shown). A similar set of binding interactions was observed with fucose at fucose-2 site (data not shown). (D) Fucose molecules at fucose-3/4 sites formed identical interactions at the dimeric interface on the P dimer. Direct hydrogen bonds to fucose were provided with the side chains of Glu359 and Lys449. A hydrophobic interaction was formed between fucose and Trp381. Water-mediated interactions (spheres) are also shown. In addition, fucose molecules at fucose-3/4 sites were connected with a hydrophobic interaction and a water-meditated interaction.

et al., 2012). Diffraction images were processed with XDS at similar resolutions (~1.8 Å) and comparable data quality for all datasets. Structures were solved by molecular replacement using Phaser using PDB-ID 3ONU as a search model and refined using Phenix.refine and Coot as previously described (Singh et al., 2015). Fucose and B-tri were added to the model at the final stages of refinement in order to reduce bias of the electron density map. Atomic coordinates and structure factors for the structures solved

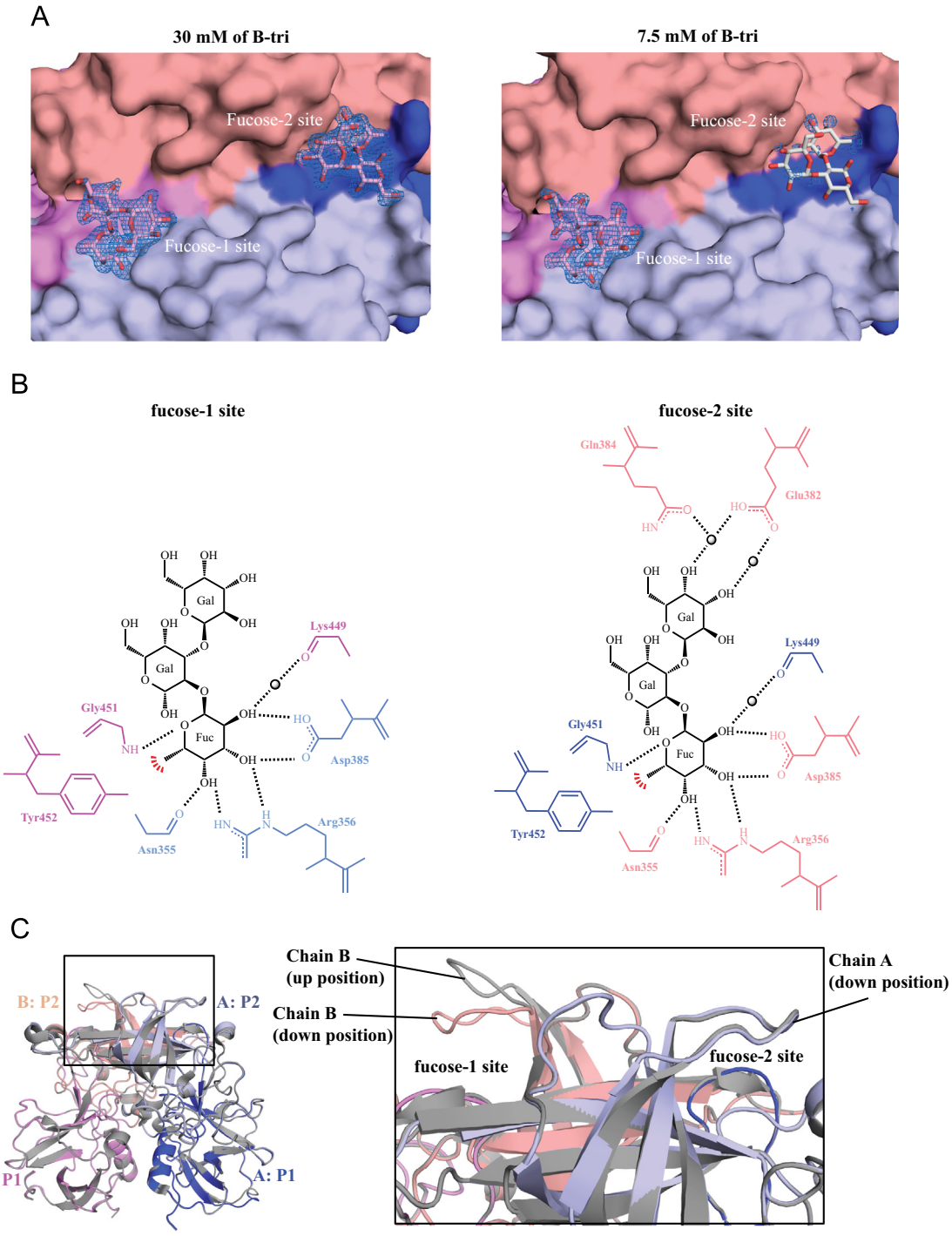


**Fig. 2.** GII.10 P domain binding interaction with B-tri. The B-tri is an α-L-fucose-(1-2)-β/α-D-galactose-(3-1)-α-D-galactose (the underlined β represents the position of the reducing end hydroxyl group, which was fixed in α position in the crystal structures). (A) A close-up surface representation of the P dimer showing the two B-tri molecules (pink sticks) bound at fucose-1/2 sites at 30 mM of B-tri (left). At 7.5 mM of B-tri (right), only one B-tri molecule (pink sticks) bound at fucose-1 site, while the fucose-2 site was unoccupied (white sticks). The simulated annealing $F_o - F_c$ omit map (blue) was contoured at 2.5σ. (B) The B-tri interactions at fucose-1 site (left) and fucose-2 site (right) at 30 mM of B-tri. The binding interactions were similar to the fucose interactions at fucose-1/2 sites (see Fig. 1C). The central Galactose (Gal) did not form any interactions with the P dimer. The terminal Gal at fucose-2 site was held by single-water-mediated interactions, while the terminal Gal at fucose-1 site was not held by single-water-mediated interactions, but double-water-mediated interactions (data not shown). (C) Superposition of the GII.10 P dimer unliganded (grey, PDB ID: 3ONU) and GII.10 P dimer B-tri$^{30\ mM}$ complex structures (colored as in Fig. 1A), showing a close-up of the Val294–Thr301 loops (chains A/B). The unliganded GII.10 P dimer showed two alternative loop positions, which were observed for other GII.10 P dimer HBGA complexes that bound HBGAs at only fucose-1 site (Hansman et al., 2011), including the GII.10 P dimer B-tri$^{7.5\ mM}$. In the GII.10 P dimer B-tri$^{30\ mM}$ complex, chain B loop was repositioned "down" at fucose-1 site.

have been deposited in the Protein Data Bank with the following PDB IDs 4Z4R, 4Z4S, 4Z4T, 4S4U, 4S4V, 4S4W, 4Z4Y, and 4Z4Z (Tables 1 and 2).

## Acknowledgments

The funding for this study was provided by the CHS Foundation and the Helmholtz-Chinese Academy of Sciences. We acknowledge the European Synchrotron Radiation Facility for provision of synchrotron radiation facilities, Protein Crystallization Platform, CellNetworks, Heidelberg for assistance with protein crystallization. We would also like to thank Thilo Stehle and Luisa Stroeh for their helpful discussions with the titration experiments.

## References

Bowler, M.W., Guijarro, M., Petitdemange, S., Baker, I., Svensson, O., Burghammer, M., Mueller-Dieckmann, C., Gordon, E.J., Flot, D., McSweeney, S.M., Leonard, G. A., 2010. Diffraction cartography: applying microbeams to macromolecular crystallography sample evaluation and data collection. Acta crystallographica. Section D, Biological crystallography 66, 855–864.

Brockhauser, S., Svensson, O., Bowler, M.W., Nanao, M., Gordon, E., Leal, R.M.F., Popov, A., Gerring, M., McCarthy, A.A., Gotz, A., 2012. The use of workflows in the design and implementation of complex experiments in macromolecular crystallography. Acta Crystallographica Section D 68, 975–984.

Bu, W., Mamedova, A., Tan, M., Xia, M., Jiang, X., Hegde, R.S., 2008. Structural basis for the receptor binding specificity of Norwalk virus. J. Virol. 82, 5340–5347.

Cao, S., Lou, Z., Tan, M., Chen, Y., Liu, Y., Zhang, Z., Zhang, X.C., Jiang, X., Li, X., Rao, Z., 2007. Structural basis for the recognition of blood group trisaccharides by norovirus. J. Virol. 81, 5949–5957.

Hansman, G.S., Biertumpfel, C., Georgiev, I., McLellan, J.S., Chen, L., Zhou, T., Katayama, K., Kwong, P.D., 2011. Crystal structures of GII.10 and GII.12 norovirus protruding domains in complex with histo-blood group antigens reveal details for a potential site of vulnerability. J. Virol. 85, 6687–6701.

Hansman, G.S., Shahzad-Ul-Hussan, S., McLellan, J.S., Chuang, G.Y., Georgiev, I., Shimoike, T., Katayama, K., Bewley, C.A., Kwong, P.D., 2012. Structural basis for norovirus inhibition and fucose mimicry by citrate. J. Virol. 86, 284–292.

Jones, M.K., Watanabe, M., Zhu, S., Graves, C.L., Keyes, L.R., Grau, K.R., Gonzalez-Hernandez, M.B., Iovine, N.M., Wobus, C.E., Vinje, J., Tibbetts, S.A., Wallet, S.M., Karst, S.M., 2014. Enteric bacteria promote human and mouse norovirus infection of B cells. Science 346, 755–759.

Lundquist, J.J., Toone, EJ.,, 2002. The cluster glycoside effect. Chem. Rev 102, 555–578.

Noble, G.T., Flitsch, S.L., Liem, K.P., Webb, S.J., 2009. Assessing the cluster glycoside effect during the binding of concanavalin A to mannosylated artificial lipid rafts. Org. Biomol. Chem. 7, 5245–5254.

Prasad, BV., Hardy, ME., Dokland, T., Bella, J., Rossmann, MG., Estes, MK., 1999. X-ray crystallographic structure of the Norwalk virus capsid. Science 286, 287–290.

Singh, B.K., Leuthold, M.M., Hansman, G.S., 2015. Human noroviruses' fondness for histo-blood group antigens. J. Virol. 89, 2024–2040.

Soisson, S.M., MacDougall-Shackleton, B., Schleif, R., Wolberger, C., 1997. The 1.6 A crystal structure of the AraC sugar-binding and dimerization domain complexed with D-fucose. Journal of molecular biology 273, 226–237.

Wimmerova, M., Kozmon, S., Necasova, I., Mishra, S.K., Komarek, J., Koca, J., 2012. Stacking interactions between carbohydrate and protein quantified by combination of theoretical and experimental methods. PloS one 7, e46032.